Supporting Information

Notch-Insensitive, Ultrastretchable, Efficient Self-Healing Supramolecular Polymers Constructed from Multiphase Active Hydrogen Bonds for Electronic Applications

JianHua Xu[1], Peng Chen[2], JiaWen Wu[1], Po Hu[1], YongSheng Fu[2], Wei Jiang[3] & JiaJun Fu[1*]

1. School of Chemical Engineering, Nanjing University of Science and Technology, Nanjing, 210094, P. R. China

2. Key Laboratory for Soft Chemistry and Functional Materials of Ministry Education, Nanjing University of Science and Technology, Nanjing, 210094, P. R. China

3. National Special Superfine Powder Engineering Technology Research Center, Nanjing University of Science and Technology, Nanjing, 210094, P. R. China

*Corresponding author. E-mail: fujiajun668@gmail.com

1. Characterization

^{1}H NMR spectra were recorded on a Bruker 300 MHz spectrometer at room temperature with tetramethylsilane (TMS) as an internal reference. ATR-FT-IR spectra were recorded using a Bruker Tensor 27 Fourier transform-infrared spectrometer equipped with a Specac Golden Gate ATR heating cell in the range of 4000-600 cm^{-1}. UV−vis transmittance spectra was recorded by a Thermo Fisher E220 spectrophotometer. SAXS measurements on polymer films were conducted on Bruker AXS NanoSTAR equipped with a microfocus X-ray source, operating at λ=0.154 nm. TGA was carried out on a Mettler 851e instrument with a heating rate of 20 °C min^{-1} in nitrogen atmosphere. GC-MS analysis was performed on a Thermo Scientific Trace 1300 gas chromatography tandem mass spectrometer equipped with the TG-5MS capillary column. was carried out in THF on PolyPore columns (Agilent) connected in series with a DAWN multiangle laser light scattering (MALLS) detector and an Optilab TrEX differential refractometer (both from Wyatt Technology). GC-MS DSC measurement was performed on a TA DSC-25 differential scanning calorimeter at the heating rate of 10 °C min^{-1}. AFM images were recorded with a Bruker Multimode 8 instrument in the tapping mode. FESEM measurements were performed with a JEOL 7800F field emission electron microscope under an acceleration voltage of 30 kV. Optical microscopy images were performed by Jiangnan MV3000 optical microscope. DVS was conducted on a TA VTI-SA Vapor sorption analyzer. Measurements were performed at different relative humidity from RH=0% to RH=95% with a interval of 5%

2. Mechanical testing

Tensile test were performed on a Shimadzu AGS-X tester. Three samples with a tensile size of 3 mm gauge length × 10 mm width × 0.8-1.3 mm thickness were tested for each polymer composition, and the average value was given. Tensile experiments were performed at room temperature (20 °C) at a strain rate of 100 mm min^{-1}, 200 mm min^{-1}, 500 mm min^{-1} and 1000 mm min^{-1}. For the cyclic tensile test, both loading and unloading process were performed at a strain rate of 100 mm min^{-1} at room temperature. For pure shear test, the length of the notch is 5 mm and the tensile rate is 100 mm min^{-1}.

DMA was measured using a TA DMA Q800 in the film tension geometry with a dynamic strain of 0.1%. Dimensions of the samples for DMA measurements were determined by a standard Vernier calliper. The length of the sample between the tensile clamps was determined by the DMA instruments itself.

Bulk rheological measurements were performed on TA AR G2 Rheometer (20 mm parallel steel plate). Frequency sweeps were performed at a strain amplitude of 0.1% by varying the frequency between 0.1 rad/s to 100 rad/s in a temperature range of -15-85 °C. The circular sample with diameters of 20 mm was glued to the plates to avoid slippage.

3. Electrochemical measurements

The electrochemical performances were examined by galvanostatic cycling using CR2032 stainless steel coin cells. The sulfur loading of the electrode was about 1.5-2.0 mg cm^{-2}. The respective PDMS-MPI-TM/MWCNTs-C/S electrode functioned as the working electrode, lithium foil as the counter

electrode, 1 M LiTFSI in a mixed solvent of DOL and DME with a volume radio of 1:1 as the electrolyte, and a monolayer PP separator as the separator. The coin batteries were charged/discharged with different current densities between 1.7 and 2.8 V on a CHI660D battery test system (Chenhua, Shanghai, China) at 25°C. EIS was measured in the frequency range of 10 mHz-100 kHz.

4. Supplementary Figures

Figure S1. Digital photograph of PDMS-MPI film. The prepared PDMS-MPU film is translucent, indicating the semi-crystalline behavior. The inserted logo reproduced with permission of Nanjing University of Science and Technology

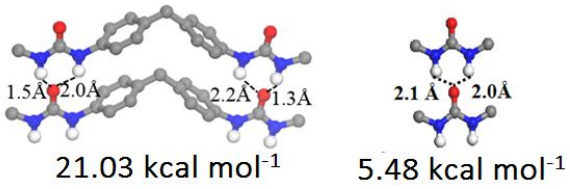

Figure S2. DFT-optimized structure of different H-bonds constructed by 4'4-methylenebis(phenyl urea) (MPU) and urea. As shown, the interaction energy of MPU-MPU linkages is larger than urea-urea dimer, indicating that the existence of aromatic rings enhance the intermolecular interactions within hard domains of PDMS-MPU.

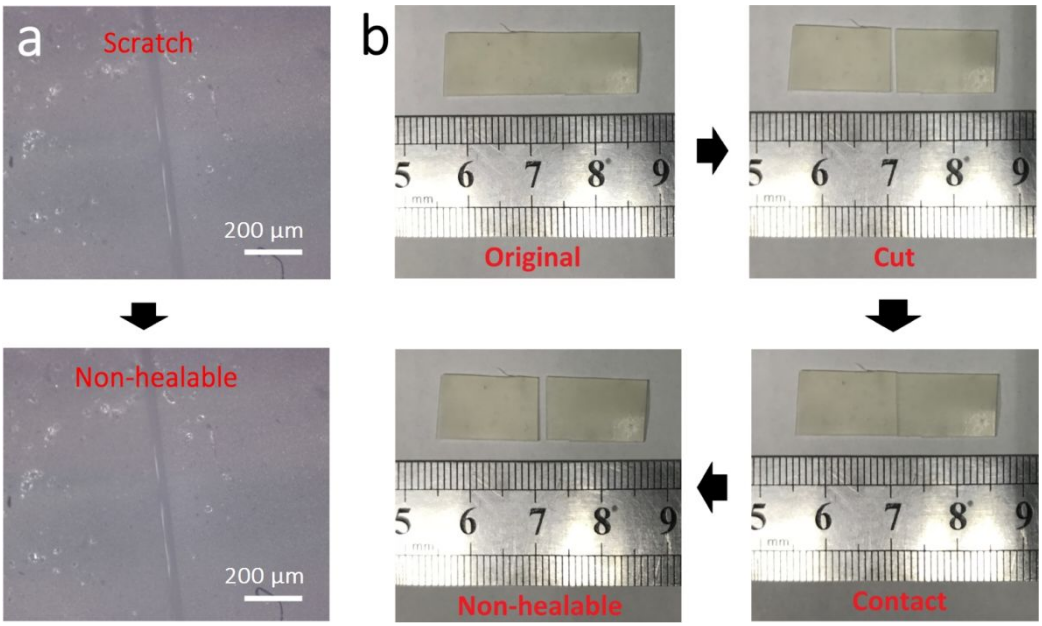

Figure S3. (a) Optical microscope images and (b) digital photograph recording the healing process of

PDMS-MPI film. As shown, PDMS-MPI film was first cut into two halves, and then the cut species were brought into contacted for healing. However, the damaged PDMS-MPI film could not restore themselves even healing for 24 h at room temperature. Meanwhile, the artificial scratch on PDMS-MPI film could also not be restored after healing for 24 h at room temperature. All of these results suggest the non-healable behavior of PDMS-MPI film.

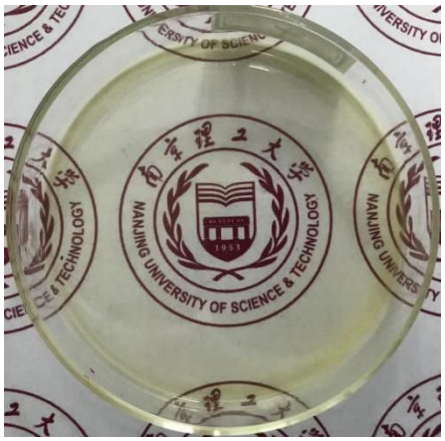

Figure S4. Digital photograph of PDMS-MPI-TM film. The prepared PDMS-MPU-TM film is totally transparent, indicating an amorphous structure. The inserted logo reproduced with permission of Nanjing University of Science and Technology.

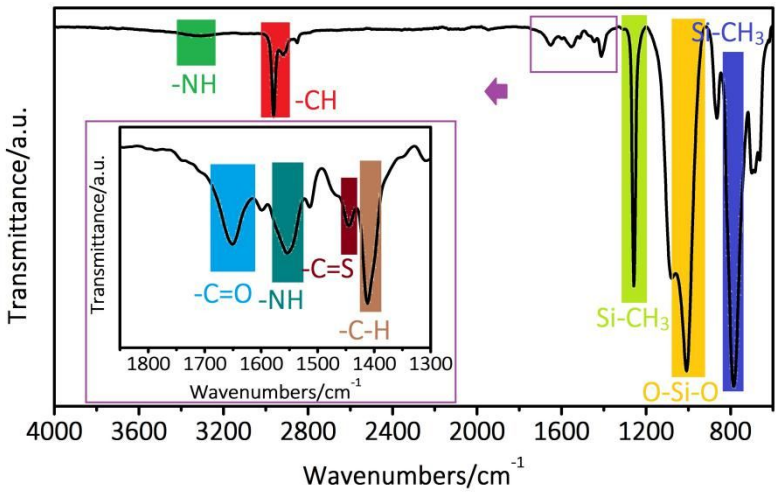

Figure S5. FT-IR spectra of the prepared PDMS-MPI-TM film. As shown, FT-IR spectra displays three characteristic peaks centered at 1652 cm^{-1}, 1598 cm^{-1}, and 1445 cm^{-1}, which are assigned to the stretching vibration of C=O from urea groups, the flexural vibrations of -NH from amino group, and the stretching vibration of C=S from thiourea groups, respectively, indicating the successful synthesis of PDMS-MPI-TM.

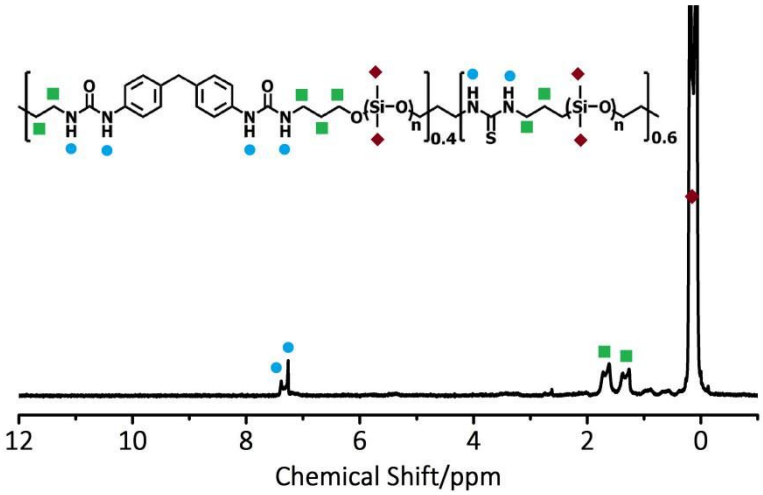

Figure S6. ^{1}H NMR spectra for PDMS-MPI-TM (300 MHz, $CDCl_3$, 298 K).

Sample	M_n (g/mol)	M_w (g/mol)	PDI (M_w/M_n)
PDMS-MPI	63380	117900	1.86
PDMS-TM	72060	119120	1.65
PDMS-MPI-TM	71640	130280	1.82
PDMS-MPI-CM	69290	119170	1.72
PDMS-HDI	79490	126380	1.59
PDMS-HDI-TM	67950	122980	1.81

Figure S7. **Summary of molecular weight for prepared polymer**. M_n is the number-average molecular weight; M_w is the weight-average molecular weight; PDI is the polydispersity index (M_w/M_n).

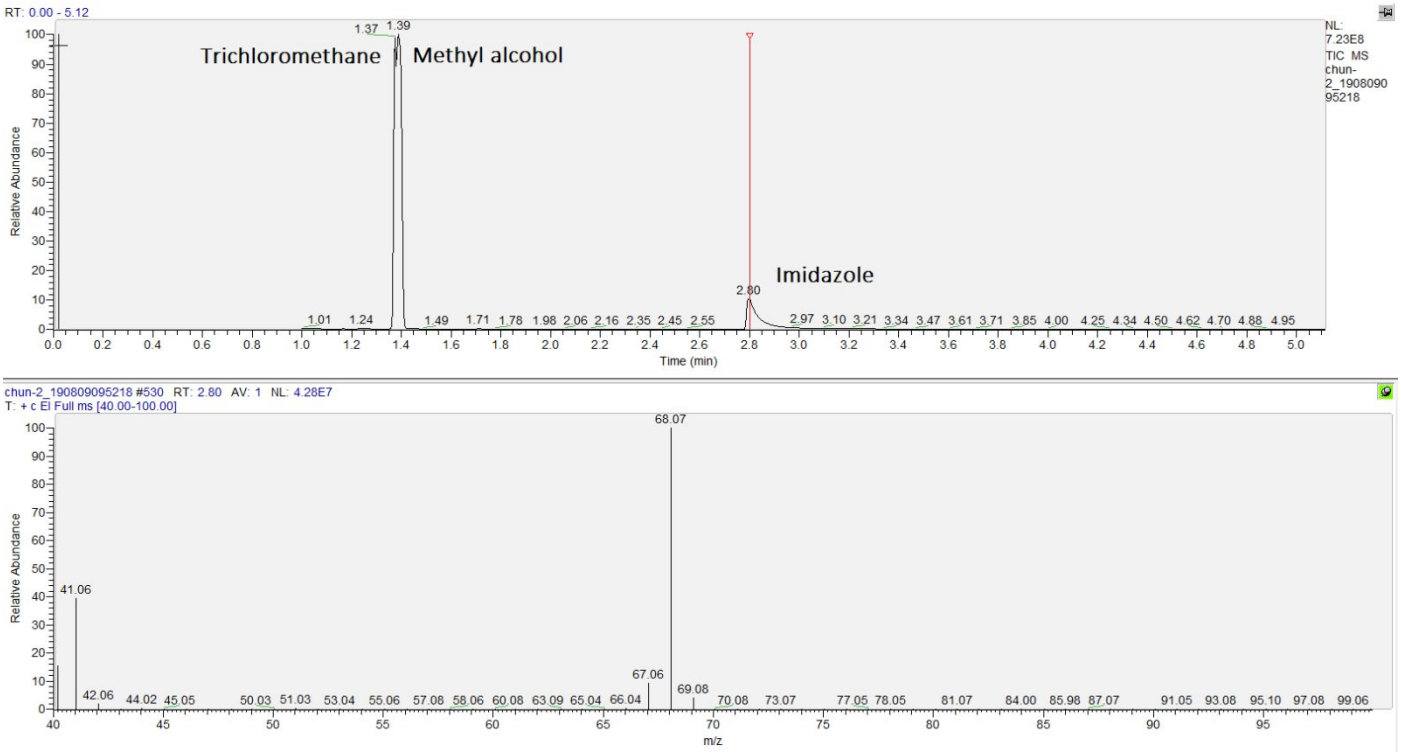

Figure S8. Gas chromatograph-mass spectrometer of the PDMS-MPI-TM polymer eluant. We employ gas chromatograph-mass (GC-MS) spectrometer to detect the presence of TM in the polymer solution after the reaction. As shown in Figure S8, there is no TM in the polymer eluent. In contrast, the imidazole component was detected. This result accords with the chemical equation (see below). It is believed that in the preparation process, TM reactants are able to completely react with amino, just like the MPI moieties. Therefore, the ratio of MPI and TM in PDMS-MPI-TM is theoretically consistent with the feed ratio.

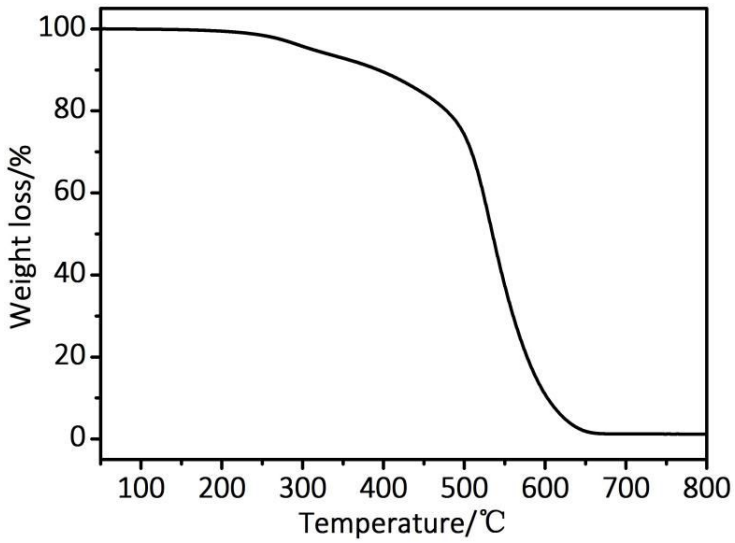

Figure S9. TG curve of PDMS-MPI-TM film. TG analysis shows that PDMS-MPI-TM film starts to lose weight at 250 °C, suggesting an excellent thermal stability.

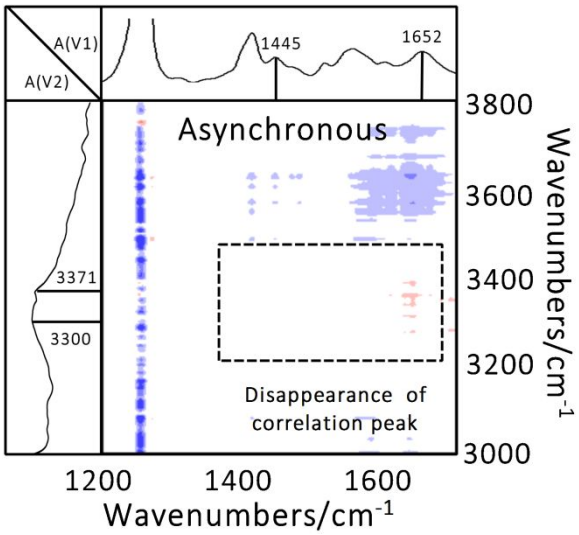

Figure S10. Asynchronous 2D correlation spectra of PDMS-MPI-TM calculated from 20-60 °C..

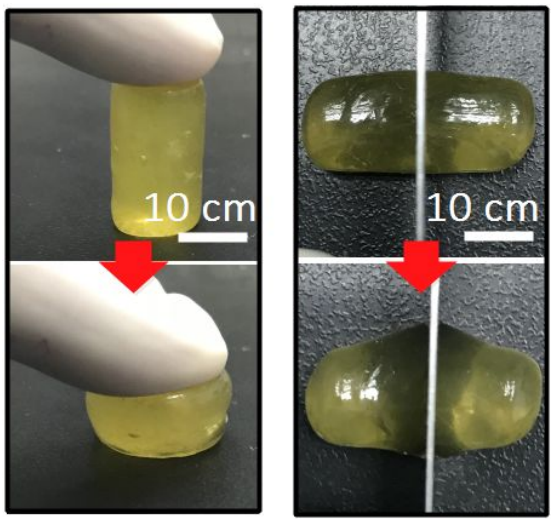

Figure S11. Photos showing that a free-standing PDMS-MPI-TM sample can not be pressed into fragmentation and easily cut into halves.

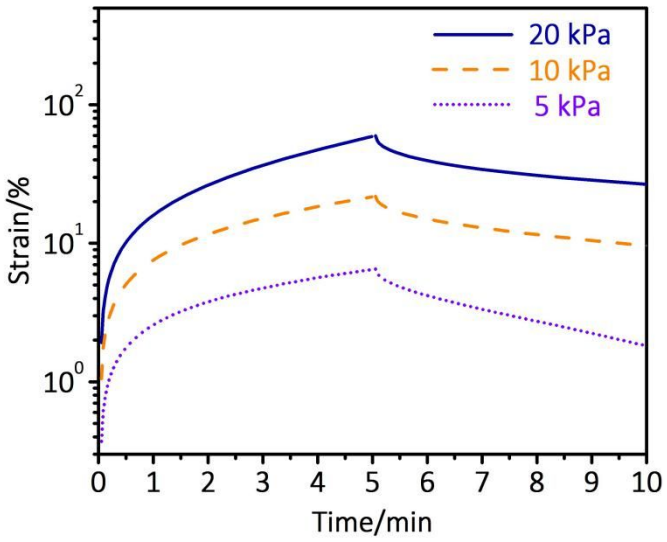

Figure S12. Creep recovery experiments performed on PDMS-MPI-TM film at varying stress. Creep recovery experiments confirm that the PDMS-MPI-TM network can sustain significant load. As shown, a stress of 5 kPa was applied of 5 min, which led to an instantaneous strain of 6.5%. Upon releasing the applied stress, the film almost completely recovered to its original dimensions with negligible residual strain (≈1.8%). For comparison, a medium stress of 10 kPa applied for the same time results in an instantaneous strain of 22%, releasing the applied stress leaves residual strain of about 9.8%. Besides, applying a high stress of 20 kPa under the same conditions led to large strain of ≈60%. Subsequently, releasing the stress left residual strain of 26%.

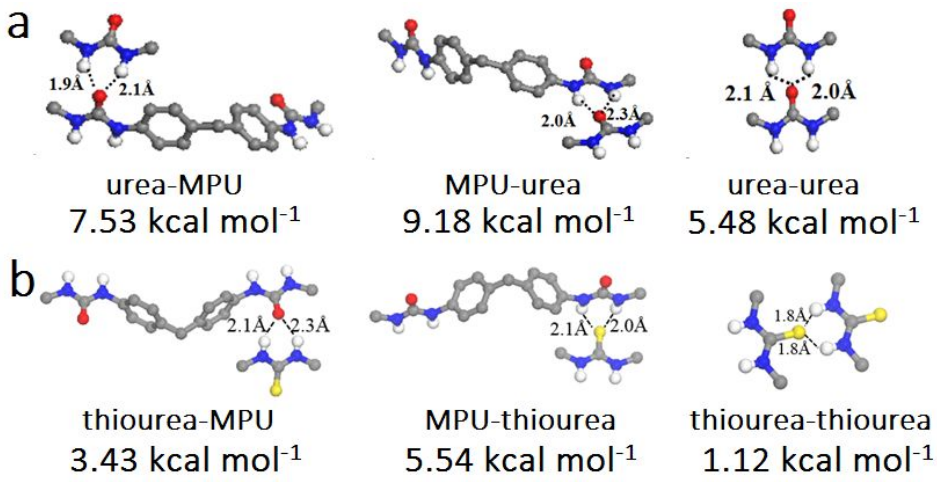

Figure S13. DFT-optimized possible configuration of H-bonds within hard domains of (a) PDMS-MPI-CM; (b) PDMS-MPI-TM.

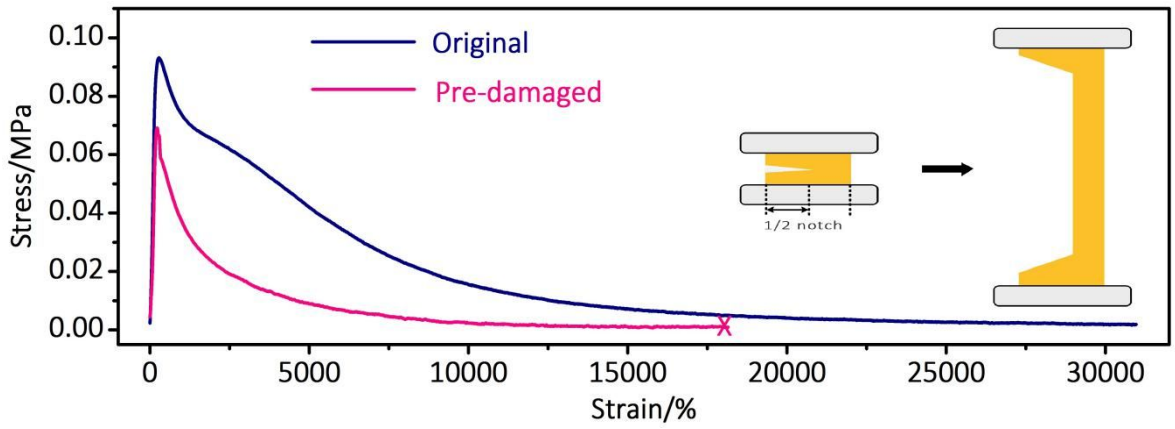

Figure S14. Tensile curves of the unnotched and notched PDMS-MPI-TM films. A notch of 5 mm in length was made in the middle of a tensile specimen of 10 mm in width and 1 mm in length. As shown, the notched PDMS-MPI-TM films could also be stretched to about 18000%, suggesting an excellent notch-insensitive ability.

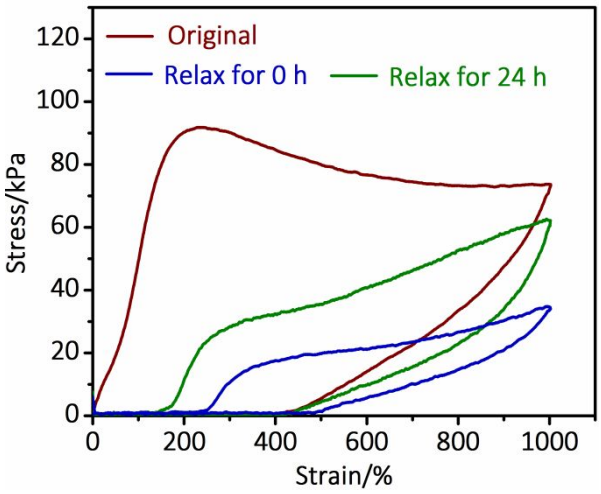

Figure S15. Cyclic loading-unloading curves of PDMS-MPI-TM film with a strain of 1000%. The stretched polymer specimen could not return back even prolonging waiting time to 24 h at an applied strain of 1000%

Figure S16. Photographs recording the self-healing process of PDMS-MPI-TM film at room temperature. As shown, a visible scratch could be autonomously restored after 4 h at room temperature without any assistance.

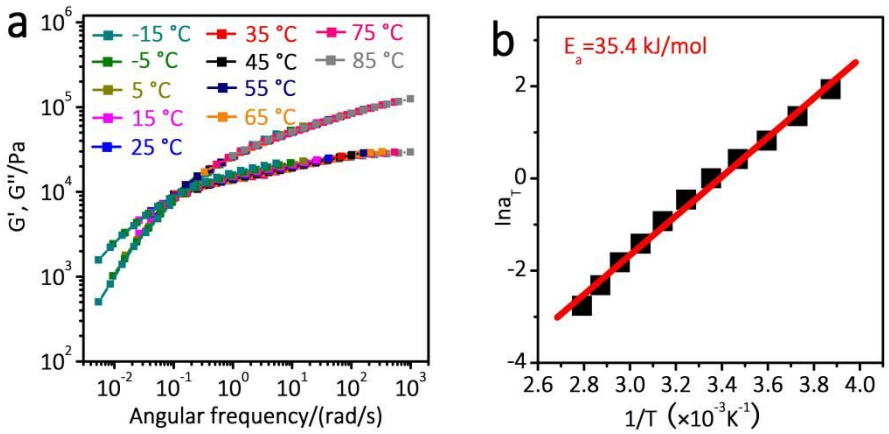

Figure S17. (a) Master curves generated using time-temperature superimposition for PDMS-MPI-TM film with a reference temperature at 25 °C; (b) Shift factor of PDMS-MPI-CM film as a function of temperature between -15 °C -85 °C.

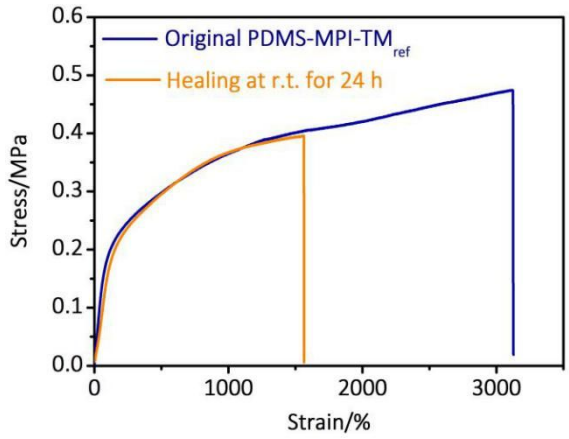

Figure S18. Tensile curves of PDMS-MPI-TM$_{ref}$ film at various healing time under room temperature. As shown, the healing efficiency of PDMS-MPI-TM$_{ref}$ was only 40% after restoring at room temperature for 24 h, which is attributed to the partial destruction of crystallization within hard domains.

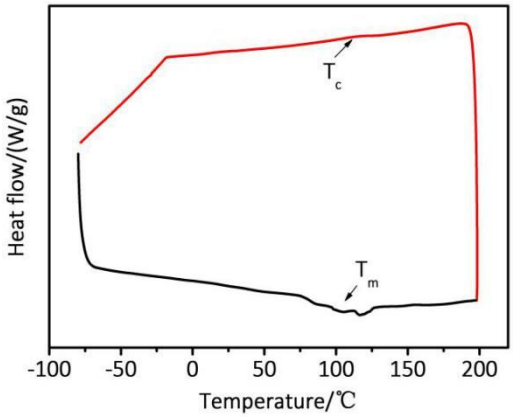

Figure S19. DSC curve of PDMS-MPI-TM$_{ref}$ film. DSC curves of PDMS-MPI-TM$_{ref}$ contains melting peak (T_m) and crystallization peak (T_c), indicating the crystallization behavior of hard domains in polymer matrix.

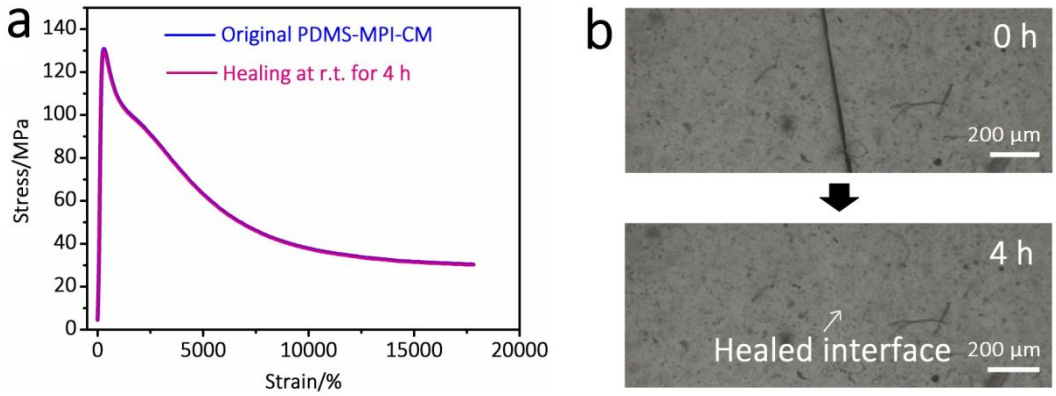

Figure S20. (a) Tensile curves and (b) optical microscope images demonstrating self-healing behavior of PDMS-MPI-CM. As shown, the complete separated PDMS-MPI-CM specimens can fully restore the mechanical properties via reconnecting only for 4 h at room temperature. Furthermore, PDMS-MPI-CM film can entirely eliminate the surface scratch after healing for 4 h at room temperature.

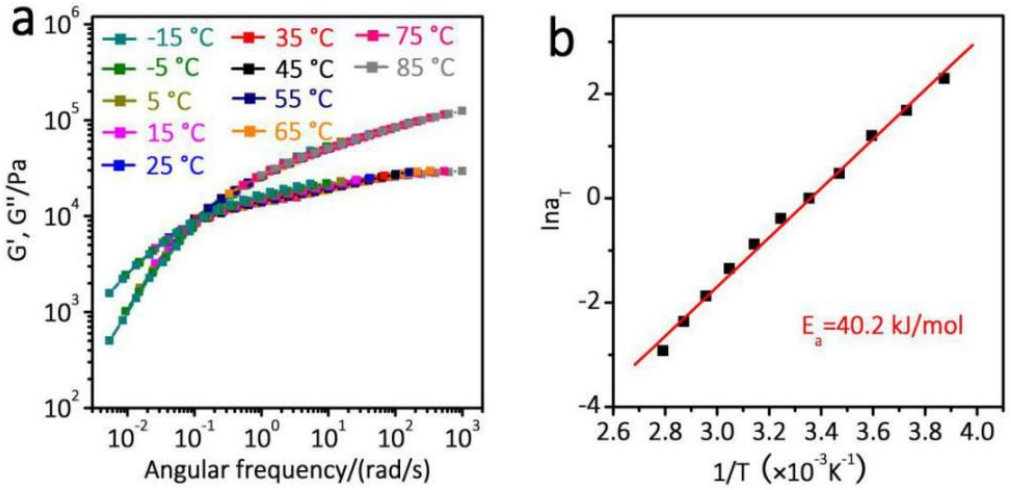

Figure S21. (a) Master curves generated using time-temperature superimposition for PDMS-MPI-CM film with a reference temperature at 25 °C; (b) Shift factor of PDMS-MPI-CM film as a function of temperature between -15 °C -85 °C. The calculated E_a value for PDMS-MPI-CM is only 40.2 kJ mol^{-1}, revealing that the multistrength H-bonds within polymer network can enable the chains to past each other easier, which is account for the fast and efficient self-healing behavior.

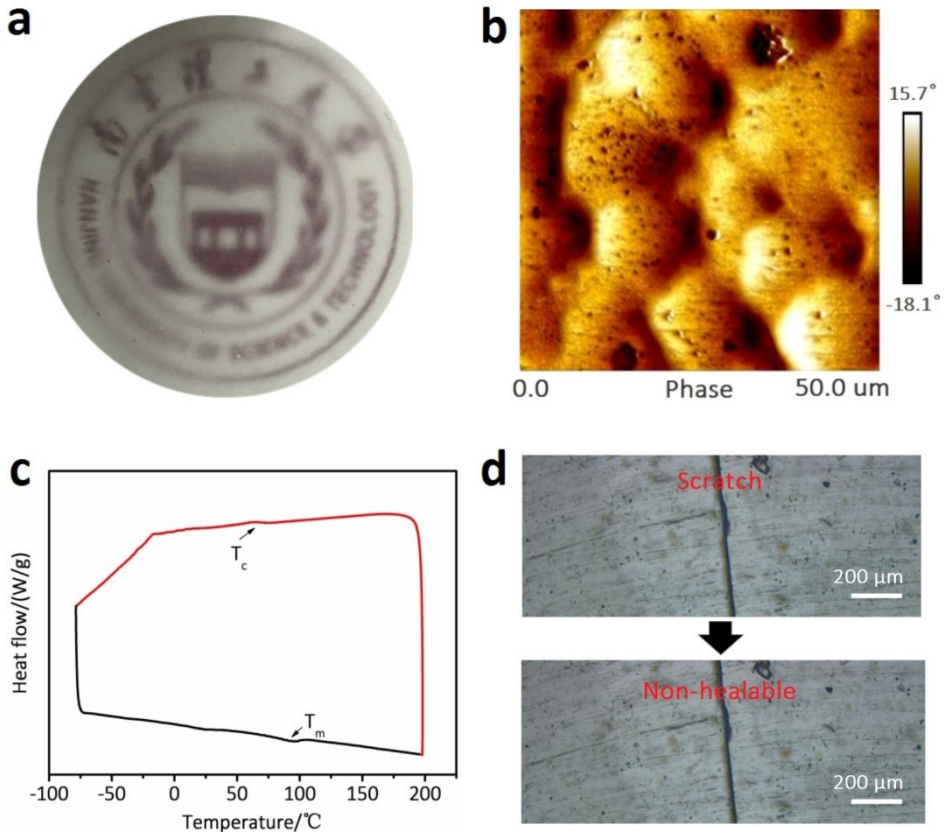

Figure S22. (a) Digital photograph, (b) AFM phase image and (c) DSC curves of PDMS-HDI film. (d) Optical microscope images recording the healing process of PDMS-MPI film. As same as the PDMS-MPI film, the as-prepared PDMS-HDI film possesses microphase-separated structure and crystallization behavior. Meanwhile, PDMS-HDI cannot eliminate the surface scratch at room temperature. The inserted logo reproduced with permission of Nanjing University of Science and Technology

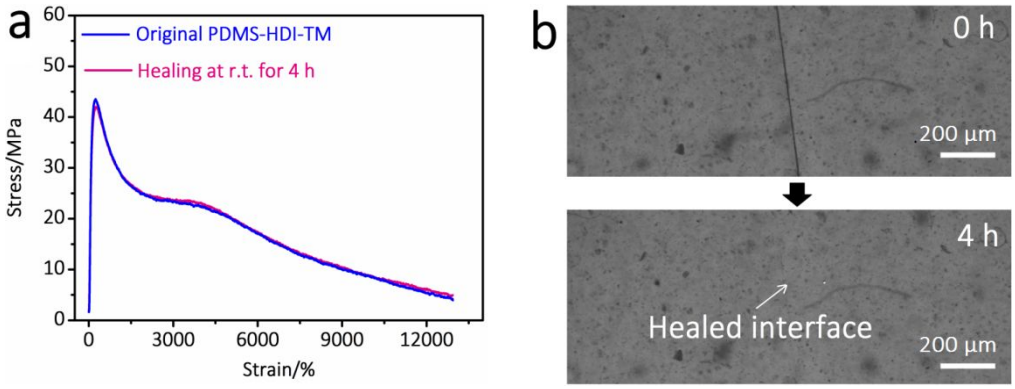

Figure S23. (a) Tensile curves and (b) optical microscope images demonstrating self-healing behavior of PDMS-HDI-TM. As shown, the complete separated PDMS-HDI-TM specimens can fully restore the mechanical properties via reconnecting only for 4 h at room temperature. Furthermore, PDMS-HDI-TM film can entirely eliminate the surface scratch after healing for 4 h at room temperature.

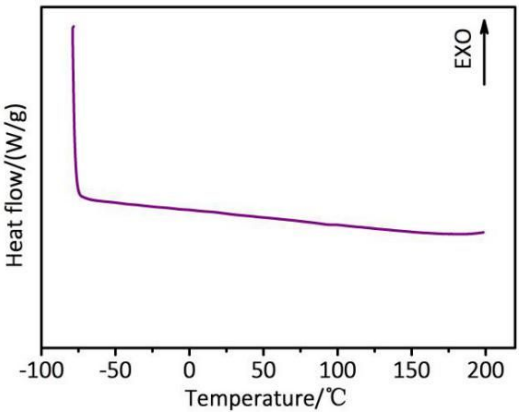

Figure S24. DSC curve of PDMS-MPI-TM film. As shown, the T_g value of PDMS-MPI-TM must be below -80 °C since there is no exothermal/endothermic signals in the DSC curve. This value is far below the room temperature, enabling sufficient re-entanglement of polymer chains during healing process.

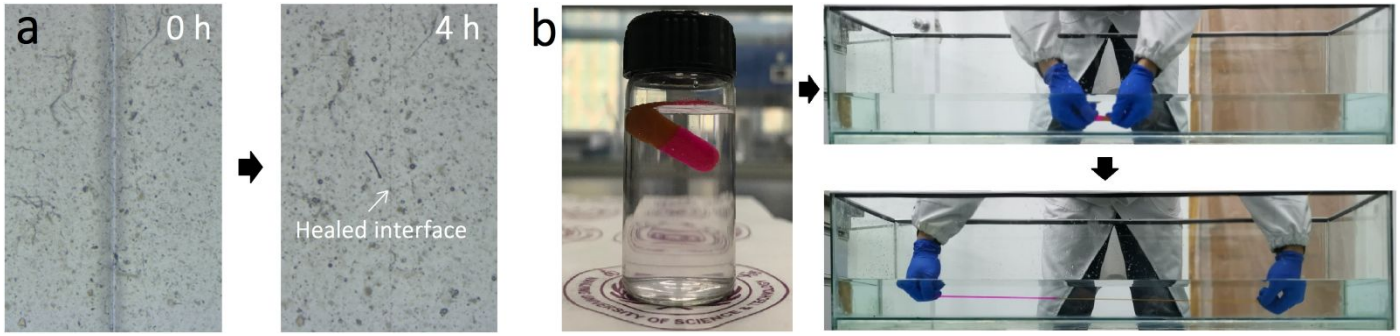

Figure S25. (a) Optical microscope images demonstrating self-healing behavior of PDMS-MPI-TM under water at room temperature; (b) Photographs showing the large stretching behavior of the underwater healed film.

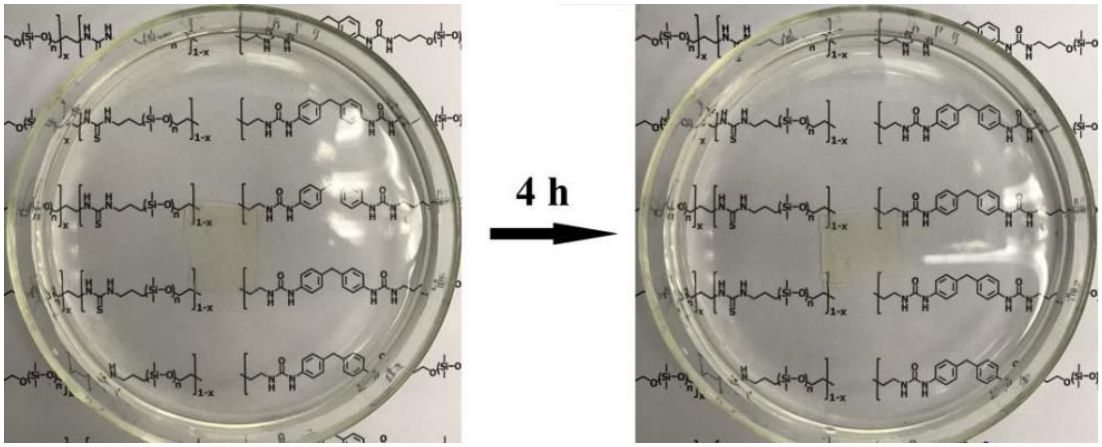

Figure S26. Photographs recording the swelling behavior of PDMS-MPI-TM film under water for 4 h. As shown Figure S25, we can see that the PDMS-MPI-TM film maintain the original shape without swelling after soaking in water for 4 h (the soaking time is same as the underwater healing time), indicating the excellent underwater stability during the healing process.

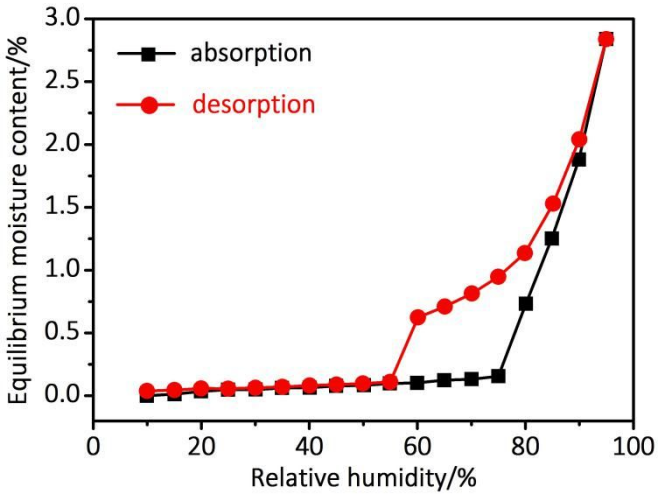

Figure S27. Water vapour adsorption-desorption isotherms for PDMS-MPI-TM film. Water vapour adsorption-desorption isotherms was employed to further quantitatively evaluate the adsorption behavior of PDMS-MPI-TM film. As shown in Figure S18, the PDMS-MPI-TM film is slightly hygroscopic that can adsorb a little water under high humidity.

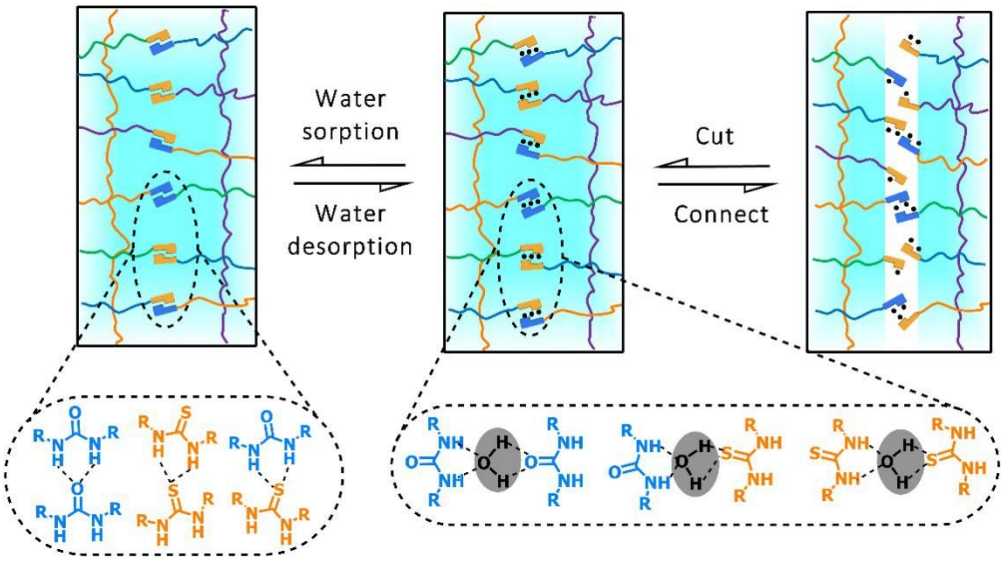

Figure S28. Schematic illustration of thiourea and urea hydrogen bonds dissociating and exchanging with water molecules during underwater healing process. A little water in PDMS-MPI-TM matrix may interact with original MPI and TM H-bonding arrays to assemble a new H-bonding system for self-healing under water.

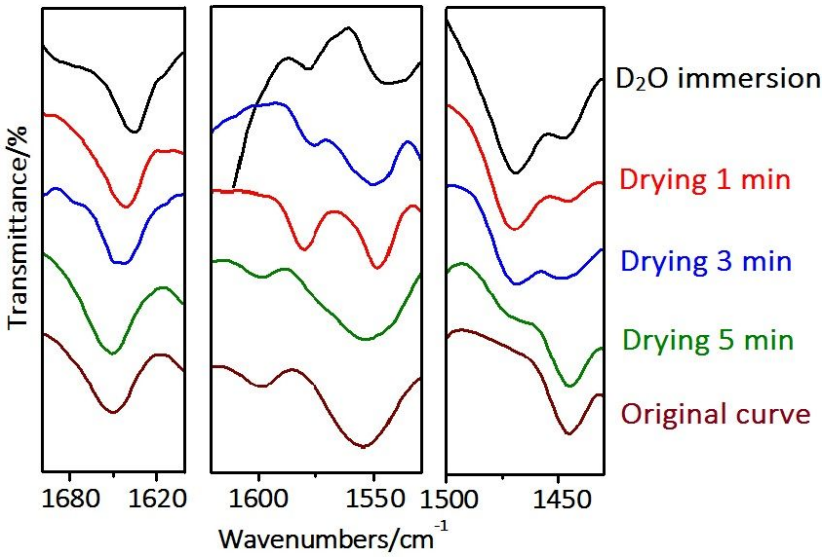

Figure S29. ATR-IR spectra of D_2O-containing PDMS-MPI-TM sample as a function of drying time. As shown, D_2O gradually evaporates from the polymer matrix, and the IR absorption peak of PDMS-MPI-TM gradually returns to their original state as the increasing of drying time, indicating the reversible process of water uptake and dehydrate.

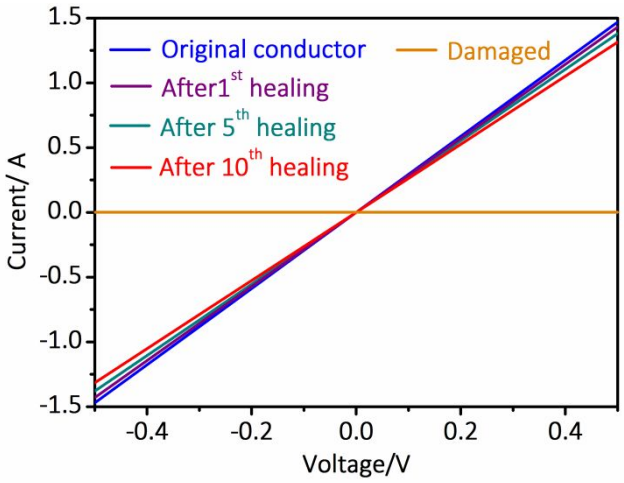

Figure S30. I-V curves of the PDMS-MPI-TM/EGaInPs conductor that underwent multiple cutting-healing cycles. As shown, the cutting-healing cycles in the same damaged region did not evidently alter electrical conductivity. Even after the 10th cycle, the electrical conductivity remained stable (pristine: 0.34Ω, after 10th healing: 0.38Ω).

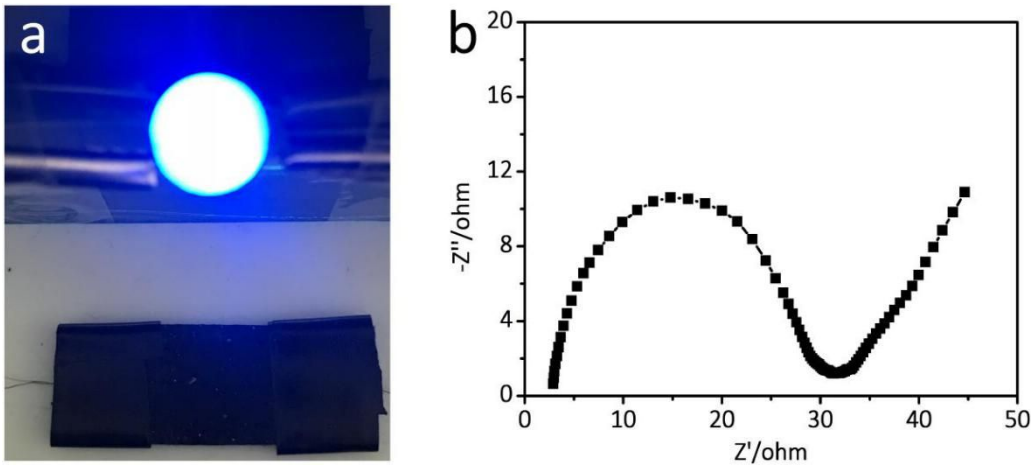

Figure S31. (a) Photograph demonstrating the electrical capability of PDMS-MPI-TM/MWCNTs-C/S composite; (b) Impedance spectroscopy measurement of PDMS-MPI-TM/MWCNTs-C/S electrode. The EIS profile indicates a decent electronic and ionic conductivity of PDMS-MPI-TM/MWCNTs-C/S electrode.

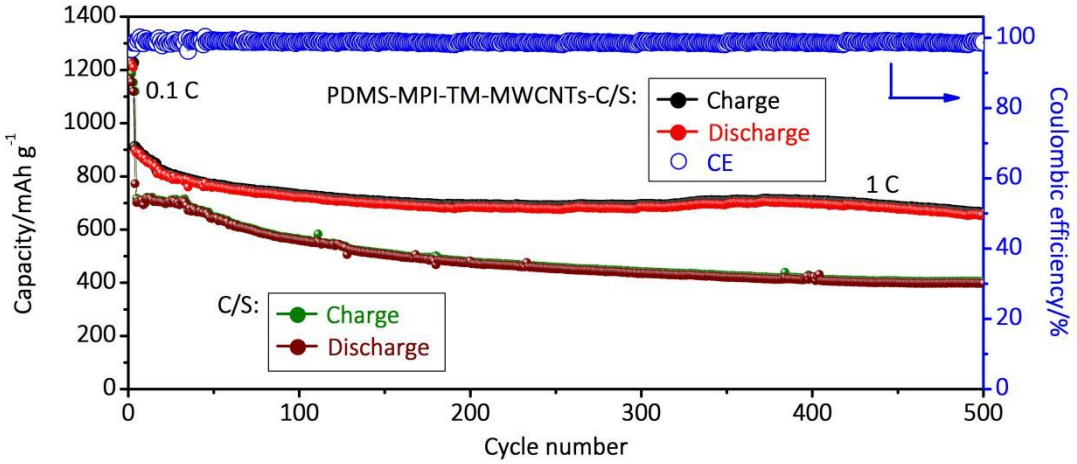

Figure S32. Cycling performance of PDMS-MPI-TM/MWCNTs-C/S electrode at 1 C (with the first 5 cycles cycled at 0.1 C for activation).

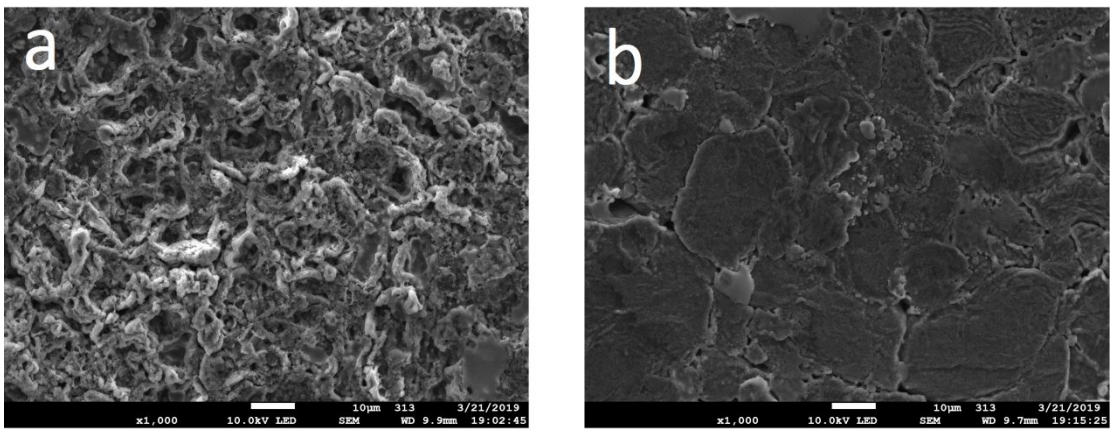

Figure S33. SEM images of Li anodes from the (a) C/S cell and the (b) PDMS-MPI-TM/MWCNTs-C/S cell after cycling for 500 cycles at 1 C. As shown, for the Li anode

obtained from the C/S battery, there was numerous uncontrolled growth of dendrite Li. In contrast, for the Li anode obtained from PDMS-MPI-TM/MWCNTs-C/S battery, a much smoother surface with only tiny dendrite Li was found after cycling, demonstrating the excellent polysulfides permeation resistance of PDMS-MPI-TM/MWCNTs-C/S layer.

Supplementary Table

Table S1. Summary of the self-healing properties of PDMS-MPI-TM film

Healing time (h)	Toughness[a] (MJ/m^3)	Self-healing efficiency[b] (%)
Original film	5.57±0.09	/
1/6	0.78±0.03	14.0%
1/3	1.94±0.03	34.8%
1	4.39±0.05	78.8%
2	5.08±0.08	91.2%
4	5.56±0.11	99.8%

[a]Toughnessis calculated by manually integrating the area under the stress-strain curve. [b]Self-healing efficiency is calculated from the ratio of tensile strength of healed films to that virgin film.

Supplementary Movie

Movie S1: This movie showed that the PDMS-MPI-TM film could be highly stretched under room temperature with a deformation rate of 100 mm min^{-1}. The film could be continuously stretched until it was up to the limited range of the tensile tester. Meanwhile, the highly stretched film could be dramatically shaken with hands and it did not rupture during this process. The thickness of the film was 1 mm. The gauge length was 3 mm and the width was 10 mm.

Movie S2: This movie showed that the control PDMS-MPI-CM film could only be stretched to 178× its original length, far inferior to PDMS-MPI-TM film.

Movie S3: This movie exhibited that the notched PDMS-MPI-TM film could be stretched to 180× its original length under room temperature with a deformation rate of 100 mm min^{-1}. The length of the notch was 5 mm.

Movie S4: This movie demonstrated the predamaged PDMS-MPI-TM/MWCNTs film with a 5 mm notch could stand 20 cycles of loading-unloading under a stain of 100% without crack propagation.